Hindawi
Abstract and Applied Analysis
Volume 2022, Article ID 6777513, 15 pages
https://doi.org/10.1155/2022/6777513

Research Article

Optimal Homotopy Asymptotic Analysis of the Dynamics of Eyring-Powell Fluid due to Convection Subject to Thermal Stratification and Heat Generation Effect

Solomon Bati Kejela[1] **and Emiru Rufo Adula**[2]

[1]*Department of Mathematics, Jimma University, Jimma, Ethiopia*
[2]*Department of Mathematics, Jimma College of Teacher Education, Jimma, Ethiopia*

Correspondence should be addressed to Solomon Bati Kejela; solomonbati@yahoo.com

Received 19 February 2022; Revised 9 August 2022; Accepted 17 August 2022; Published 23 September 2022

Academic Editor: Devendra Kumar

In the present study, the effect of thermal stratification and heat generation in the boundary layer flow of the Eyring-Powell fluid over the stratified extending surface due to convection has been investigated. The governing equations of the flow are transformed from partial differential equations into a couple of nonlinear ordinary differential equations via similarity variables. The optimal homotopy asymptotic method (OHAM) is used to acquire the approximate analytical solution to the problems. Impacts of flow regulatory parameters on temperature, velocity, skin friction coefficient, and Nusselt number are examined. It is discovered that the fluid velocity augments with a greater value of material parameter E, mixed convection parameter λ, and material fluid parameter σ. The result also revealed that with a higher value of the Prandtl number Pr and the stratified parameter ε, the temperature and the velocity profile decreases, but the opposite behavior is observed when the heat generation/absorption parameter γ increases. The results are compared with available literature and are in good harmony. The present study has substantial ramifications in industrial, engineering, and technological applications, for instance, in designing various chemical processing equipment, distribution of temperature and moisture over agricultural fields, groves of fruit trees, environmental pollution, geothermal reservoirs, thermal insulation, enhanced oil recovery, and underground energy transport.

1. Introduction

The study of the dynamics of non-Newtonian fluids has inconceivable importance on account of its numerous biological, industrial, and engineering applications. They have a vital role in material production, mixture, paper coating, bioengineering, oil repository designing, petroleum production, food engineering, chemical engineering, and the study of electroosmatic flow, blood flow, etc. [1–8]. Non-Newtonian fluid can be found in numerous materials for example in shampoos, paints, cosmetic productions, body fluids, grease, and animal blood to name a few. Several models including the Eyring-Powell model (one among the non-Newtonian fluid models) have been proposed by different scientists for the analysis of dynamics of non-Newtonian fluids. The Eyring-Powell model is derived from the kinetic molecular theory of liquids rather than empirical relation and properly shows the Newtonian behavior at low and high shear rates; owing to this, it gained the attention of many scholars. This class of fluid does not have constant viscosity with temperature alterations [9–13].

The Eyring-Powell fluid model has essential applications in designing various chemical processing equipment, distribution of temperature and moisture over agricultural fields, groves of fruit trees, environmental pollution, geothermal reservoirs, thermal insulation, enhanced oil recovery, and underground energy transport [11]. The Eyring-Powell model with heat transfer plays a crucial role in diverse industrial, geophysical, and natural processes. The understanding of the heat transfer effect in a variety of materials and boundary layer flow overstretching sheets is also imperative

as heat has substantial applications in diverse power station engineering, biological phenomena, and industrial branches like paper manufacture, metal extrusion, and bubble absorption [14–18].

Heat and mass transfer in the Eyring-Powell liquid model undertakes an essential role in the procedures which comprise the creation and spread of haze, plotting of mixture handling instrumentation, environmental pollution, drying of porous slides, raised oil recuperation, warm protection, and underground energy transport [19–21]. Ishaq et al. [22] explored the 2D nanofluid film stream of the Eyring-Powell liquid with changeable heat conduction in the existence of MHD over the unsteady permeable extending sheet and asserted that the porosity parameter lessens the movement of the fluid.

Hayat et al. [23] conducted a study on MHD nonlinear extending flow of the Eyring-Powell nanofluid, where a zero nanoparticle mass flux stipulation was applied at the sheet. Their finding illustrates that with magnetic parameters, skin friction coefficient raises though the heat transmits rate at the surface declines. The heat and mass transfer analysis of non-Newtonian fluid overstretching sheets has been done by different scholars; Megahed et al. [24] conducted a study on heat transfer for MHD fluid as a result of the unsteady stretching plate with extended heat flux by varying viscosity and thermal conductivity with temperature; Reddy et al. [25] and Megahed and Gnaneswara [26] have also investigated the heat and mass transfer of different non-Newtonian flow across a stretched sheet.

Mixed convection flow plays a significant role, for example, in air limit layer flows, atomic reactors, solar gatherers, and in electronic hardware, just to name a few. Wubshet and Temesgen [19] used Cattaneo–Christov heat and mass flux model to inspect the mixed convection flow of the Eyring-Powell nanofluid through a porous medium on a linearly extending sheet in the company of permeability and Joule heating effects. They noticed that with the advanced value of the Eyring-Powell fluid parameter, the fluid velocities, local Nusselt number, and skin friction coefficient promotes. Malik et al. [27] have examined a mixed convection flow for the MHD Eyring-Powell fluid over the extending plate solving the problem numerically by the shooting method. Their outcome indicates swelling of the Eyring-Powell material parameter results in a meaningful decrease in both heat and mass transfer. Moreover, Rahimi et al. [28] presented a collocation method solution for an Eyring-Powell fluid flow over a prolonging plate. They found that the velocity enhances with mounting the Eyring-Powell fluid material parameter, but the opposite behavior is observed when the fluid material parameter is augmented.

Stratification plays a vigorous role in several industrial and natural phenomena. Owing to its wide uses in fluid mechanics, several investigators studied the stratification phenomenon. Zubair et al. [29] investigated the attributes of a chemical reaction and twofold stratification in the Eyring-Powell fluid flow persuaded by a nonlinear prolonging plate with changeable thickness. They confirmed the temperature decline with thermal stratified parameters; Salahuddin et al. [30] inspected the vital aspects of the stratification procedure with linear convection. They discovered that with an enhanced value of the thermal stratification parameter the velocity, the temperature profile reduces. Hayat et al. [31] examined the MHD effect for heat and mass transfer through the double stratified sheet. They reported that thermal and solutal stratification parameters have a conflicting effect on temperature distributions. Furthermore, Ogunseye et al. [32] examined the effect of thermal radiation on the flow and heat transfer of the Eyring-Powell nanofluid. The understanding of the heat generation/absorption effect of boundary layer flow is also crucial in different fields of study and applications. Owing to this, a lot of scholars [33–35] conducted a study on the heat generation effect on boundary layer flow and heat transfer due to different non-Newtonian fluids. The study of the boundary layer flow of the Eyring-Powell fluid over a stretching surface plays a vital role in industrial applications. A stretching surface has abundant significance in numerous industrial applications including electronic chips, fiber yarn, polymer industries, and glass blowing.

Motivated by the above significant studies, we consider the problem of the Eyring-Powell fluid flow over a stratified stretching surface subject to mixed convection and heat generation/absorption effect. The problem has plenty of applications in various fields of science and engineering but it has not been analytically investigated so far. Moreover, the effect of heat generation and thermal stratification on the flow of the fluid under consideration is not investigated. Hence, the novelties of the current work are the investigation of the heat generation and thermal stratification effects in the boundary layer flow of the Eyring-Powell fluid over the stratified extending surface due to convection, the use of OHAM for solving the problem, and the analysis of effects of different parameters on velocity and temperature of the considered fluid. The effectiveness and reliability of the proposed method have been proved in many research articles, and it is used for solving both nonlinear and linear problems by several authors [34, 36–38].

2. Mathematical Formulation

In the model, a two-dimensional incompressible steady boundary layer mixed convection flow of the Eyring-Powell fluid over the stratified extending surface has been pondered. The sheet is elongated at invariable speed $u_w = a$ x along the x *-axis* in a vertical direction and the fluid temperature at and far away from the plate surface is given, respectively, by T_w and T_∞. The influence of heat generation/absorption is considered in the energy equation. The geometric representation of the problem under consideration and the coordinate system are displayed in Figure 1.

Applying the boundary layer estimation the governing equation of the problem is condensed into the following form (see [21, 39, 40]):

Continuity equation:

$$\frac{\partial u}{\partial x} + \frac{\partial v}{\partial y} = 0. \tag{1}$$

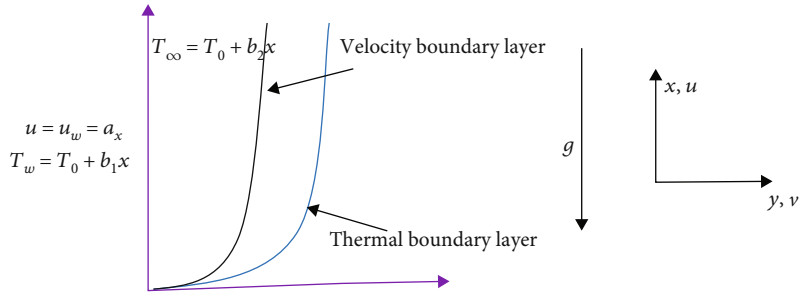

Figure 1: Physical model of the problem.

Momentum equation:

$$u\frac{\partial u}{\partial x} + v\frac{\partial u}{\partial y} = \left(\upsilon + \frac{1}{\rho\beta c} - \frac{1}{2\rho\beta c^3}\left(\frac{\partial u}{\partial y}\right)^2\right)\frac{\partial^2 u}{\partial y^2} + g\beta(T - T_\infty), \tag{2}$$

where u and v, x and y, respectively, represent the horizontal and vertical components of fluid velocity and the coordinate system, β and c are the dimensional Eyring-Powell fluid material parameters, and υ, g represent kinematic viscosity and gravitational acceleration, respectively.

Energy equation:

$$u\frac{\partial T}{\partial x} + v\frac{\partial T}{\partial y} = \frac{k}{\rho c_p}\frac{\partial^2 T}{\partial y^2} + \frac{Q}{\rho c_p}(T - T_\infty). \tag{3}$$

The corresponding boundary conditions of the governing flow problem are (see [16, 31]) as follows:

$$\left.\begin{aligned} &u = u_w = ax, v = 0, T = T_w = T_0 + b_1 x \text{ at } y = 0 \\ &u \longrightarrow 0, T \longrightarrow T_\infty = T_0 + b_2 x \text{ as } y \longrightarrow \infty \end{aligned}\right\}, \tag{4}$$

where a is a linear stretching rate, b_1 and b_2 are positive dimensional constants, and T_0 is the stretching sheet reference temperature.

To make the arithmetical analysis simple, we convert Equations (1)–(4) into ODEs, by introducing the stream function $\psi(x, y)$, such that

$$u = \frac{\partial \psi}{\partial y}, \tag{5}$$

$$v = -\frac{\partial \psi}{\partial x}, \tag{6}$$

where

$$\psi = \sqrt{av}xf(\eta). \tag{7}$$

The dimensionless similarity variable η, stream function $f(\eta)$, and temperature $\theta(\eta)$ are defined as follows (see [21, 39, 40]):

$$\eta = y\sqrt{\left(\frac{a}{\upsilon}\right)}, \tag{8}$$

$$\theta(\eta) = \frac{T - T_\infty}{T_w - T_0}, \tag{9}$$

where $T = b_1\theta x$ and $T_\infty = T_0 + b_2 x$.

Now, Equation (1) is identically pleased with u and v of Equation (5). Furthermore, using Equation (5) and (8), Equations (2) and (3) become converted into the following ODEs:

$$(1+\epsilon)f''' + ff'' - \sigma\epsilon\left(f''\right)^2 f''' - \left(f'\right)^2 + \lambda\theta = 0, \tag{10}$$

$$\theta'' + \mathrm{Pr}f\theta' + \mathrm{Pr}\gamma\theta - \mathrm{Pr}f'\theta - \mathrm{Pr}e_1 f' = 0, \tag{11}$$

where $\epsilon = 1/\rho\beta c\upsilon, \sigma = u_w^2 a/2\upsilon c^2, \lambda = g\beta b_1/a^2, \mathrm{Pr} = \mu c_p/k, \gamma = Q/ac_p\rho$, and $e_1 = b_2/b_1$ represent a material parameter, fluid parameter, mixed convection parameter, Prandtl number, heat generation/absorption parameter, and thermal stratification parameter, respectively. Moreover, the prescribed side conditions Equation (4) become reduced to

$$\left.\begin{aligned} &f(0) = 0, f'(0) = 1, \theta(0) = 1 - e_1 \text{ at } y = 0 \\ &f'(\eta) = 0, \theta(\eta) = 0 \text{ as } \eta \longrightarrow \infty \end{aligned}\right\}. \tag{12}$$

The physical quantities of interest: local skin friction coefficient C_f and the Nusselt number Nu, are described as follows (see [30, 40]):

$$C_f = \frac{\tau_w}{\rho u_w^2}, \tag{13}$$

$$\mathrm{Nu} = \frac{xq_w}{k(T_w - T_\infty)}, \tag{14}$$

where u_w represents free stream speed, τ_w and q_w given by (see [21])

$$\tau_w = \left(\left(\mu + \frac{1}{\beta c}\right)\frac{\partial u}{\partial y} - \frac{1}{6\beta c^3}\left(\frac{\partial u}{\partial y}\right)^3\right)\Bigg|_{y=0}, q_w = -k\left(\frac{\partial T}{\partial y}\right)\Bigg|_{y=0}, \tag{15}$$

denote skin shear stress on a surface and heat flux at the surface.

From Equations (5), (8), (13), and (15), we obtain

$$\begin{aligned}&\sqrt{\mathrm{Re}_x}C_f = (1+\epsilon)f''(0) - \frac{1}{3}\epsilon\sigma\left(f''(0)\right)^3,\\&\left(\sqrt{\mathrm{Re}_x}\right)^{-1}\mathrm{Nu} = -\theta'(0),\end{aligned} \tag{16}$$

where $\mathrm{Re}_x = xu_w/\upsilon = ax^2$ denotes the Reynolds number and x is the distance from the reference point at which a boundary layer begins to form.

3. Solution of the Problem via the OHAM

Employing the basic principle of OHAM on Equations (10) and (11), we construct the homotopy equation:

$$\left.\begin{aligned}(1-p)(1+\epsilon)f''' &= H_1(p)\left[(1+\epsilon)f''' + ff'' - \sigma\epsilon f'^2 f''' - f'^2 + \lambda\theta\right]\\(1-p)\left(\theta''\right) &= H_2(p)\left[\theta'' + \mathrm{Pr}f\theta' - \mathrm{Pr}f'\theta + \mathrm{Pr}\gamma\theta - \mathrm{Pr}\varepsilon f'\right]\end{aligned}\right\}, \tag{17}$$

where $p \in [0, 1]$ and $f, \theta, H_1(p), H_2(p)$ are expanded as follows:

$$\begin{aligned}&f = f_0 + pf_1 + p^2f_2 + p^3f_3, \theta = \theta_0 + p\theta_1 + p^2\theta_2 + p^3\theta_3,\\&H_1(p) = pc_1 + p^2c_2 + p^3c_3, H_2(p) = pc_4 + p^2c_5 + p^3c_6,\end{aligned} \tag{18}$$

where $H_1(p)$ and $H_2(p)$ are nonzero ancillary functions for $p \neq 0$ and zero for $p = 0$. Using Equation (18) in Equation (17) and collecting like terms based on powers of p, we get the next zero-, first-, second-, and third-order problems with their boundary conditions.

The zeroth-order problem:

$$\begin{cases}f_0'''(\eta) = 0,\\ \theta_0''(\eta) = 0.\end{cases} \tag{19}$$

Boundary conditions:

$$\begin{aligned}&f_0(0) = 0, f_0'(0) = 1, \theta_0(0) = 1 - e_1,\\&f_0'(\eta) = 0, \theta_0(\eta) = 0 \text{ as} \eta \longrightarrow \infty.\end{aligned} \tag{20}$$

The solution for Equation (19) with BCs (20) is

$$\begin{cases}f_0(\eta) = \eta\left(1 - \dfrac{\eta}{20}\right),\\ \theta_0(\eta) = (1-\varepsilon)\left(1 - \dfrac{\eta}{10}\right).\end{cases} \tag{21}$$

The 1st-order problem:

$$\begin{cases}f_1'''(\eta, a_1) = \dfrac{a_1}{1+\epsilon}\left(f_0f_0'' - f_0'^2 + \lambda\theta_0\right),\\ \theta_1''(\eta, b_1) = \mathrm{Pr}b_1\left(f_0\theta_0' - f_0'\theta_0 + \gamma\theta_0 - \varepsilon f_0'\right).\end{cases} \tag{22}$$

Boundary conditions:

$$\begin{cases}f_1(0) = 0, f_1'(0) = 0, \theta_1(0) = 0,\\ f_1'(\eta) = 0, \theta_1(\eta) = 0 \text{ as} \eta \longrightarrow \infty.\end{cases} \tag{23}$$

Solution for Equation (22) with BC Equation (23) is

$$\begin{aligned}f_1(\eta, a_1) &= \frac{a_1}{(1+\epsilon)}\left[\frac{-\eta^5}{12000} + \frac{\eta^4}{240} - \frac{\eta^3}{6} + \frac{15}{8}\eta^2\right.\\&\quad\left. + \frac{\lambda}{3}(e_1 - 1)\left(\frac{\eta^4}{80} - \frac{\eta^3}{2} + 5\eta^2\right)\right),\\\theta_1(\eta, b_1) &= \frac{\mathrm{Pr}b_1}{2}\left[(\varepsilon - 1)\left(\frac{\eta^4}{1200} - \frac{\eta^3}{30} + \eta^2 - \frac{15\eta}{2}\right)\right.\\&\quad\left. + \left(\eta^2 - \frac{\eta^3}{30} - \frac{20\eta}{3}\right)(\gamma - \gamma\varepsilon - \varepsilon)\right].\end{aligned} \tag{24}$$

The 2nd-order problem:

$$\begin{cases}f_2'''(\eta, a_1, a_2) = (1 + a_1)f_1''' + \dfrac{1}{(1+\epsilon)}\left[\begin{array}{c}a_1f_0f_1'' + f_0''(a_2f_0 + a_1f_1) - \sigma\epsilon a_1f_0'^2f_1'''\\ -\left(2a_1f_0'f_1' + a_2f_0'^2\right) + \lambda(a_1\theta_1 + a_2\theta_0)\end{array}\right],\\ \theta_2''(\eta, c_4, c_5) = (1 + b_2)\theta_1'' + \mathrm{Pr}\left[\begin{array}{c}b_1\left(f_0\theta_1' + f_1\theta_0'\right) + b_2f_0\theta_0' - b_1\left(f_1'\theta_0 + f_0'\theta_1\right)\\ -b_2f_0'\theta_0 + \gamma(b_1\theta_1 + b_2\theta_0) - \varepsilon\left(b_1f_1' + b_2f_0'\right)\end{array}\right].\end{cases} \tag{25}$$

Boundary conditions:

$$\begin{cases} f_2(0) = 0, f_2{}'(0) = 0, \theta_2(0) = 0, \\ f_2{}'(\eta) = 0, \theta_2(\eta) = 0 \text{ as } \eta \longrightarrow \infty. \end{cases} \tag{26}$$

The solution for the problem is

$$\begin{aligned} & f_2(\eta, a_1, a_2) \\ &= \frac{(1+a_1)a_1}{(1+\epsilon)} \left[\frac{-\eta^5}{12000} + \frac{\eta^4}{240} - \frac{\eta^3}{6} + \frac{15\eta^2}{8} + \lambda(1-\varepsilon) \right. \\ &\quad \cdot \left. \left(\frac{\eta^3}{2} - \frac{\eta^4}{240} - \frac{5\eta^2}{3} \right) \right] + \frac{5a_{1^2}}{(1+\epsilon)^2} \left[\frac{\eta^8}{4032000} + \frac{\eta^6}{1200} \right. \\ &\quad - \frac{\eta^7}{50400} - \frac{19\eta^5}{960} + \frac{5\eta^4}{32} - \frac{275\eta^2}{336} + \lambda(1-\varepsilon) \\ &\quad \cdot \left. \left(\frac{7\eta^5}{360} - \frac{\eta^6}{1200} - \frac{5\eta^4}{36} + \frac{\eta^7}{84000} \right) \right] + \frac{1}{(1+\epsilon)} \\ &\quad \cdot \left[\frac{a_2}{10} \left(\frac{\eta^5}{1200} - \frac{\eta^4}{24} + \frac{25\eta^2}{4} \right) - \frac{{a_1}^2}{10(1+\epsilon)} \left(\frac{-\eta^8}{4032000} \right. \right. \\ &\quad + \frac{\eta^7}{50400} - \frac{\eta^6}{720} + \frac{\eta^5}{32} - \frac{19\eta^2}{56} + \lambda(1-\varepsilon) \left(\frac{\eta^6}{720} \right. \\ &\quad \left. \left. \left. - \frac{\eta^7}{50400} - \frac{\eta^5}{12} + \frac{3125\eta^2}{18} \right) \right) \right] + \frac{-\sigma \in {a_1}^2}{100(1+\epsilon)^2} \left[\frac{-\eta^5}{12000} \right. \\ &\quad \left. + \frac{\eta^4}{240} - \frac{\eta^3}{6} + \frac{15\eta^2}{8} + \lambda(1-\varepsilon) \left(\frac{\eta^3}{6} - \frac{\eta^4}{240} - \frac{5\eta^2}{3} \right) \right] \\ &\quad + \frac{\lambda a_2}{(1+\epsilon)} (1-\varepsilon) \left(\frac{\eta^3}{6} - \frac{\eta^4}{240} - \frac{5\eta^2}{3} \right) - \frac{2{a_1}^2}{(1+\epsilon)^2} \left(\frac{-\eta^7}{504000} \right. \\ &\quad + \frac{\eta^6}{7200} - \frac{\eta^5}{120} + \frac{5\eta^4}{32} - \frac{125\eta^2}{9} + \lambda(1-\varepsilon) \left(\frac{\eta^5}{120} \right. \\ &\quad \left. \left. - \frac{\eta^6}{7200} - \frac{5\eta^4}{36} + \frac{100\eta^2}{9} \right) \right) + \frac{2{a_1}^2}{10(1+\epsilon)^2} \left[\frac{-\eta^8}{806400} \right. \\ &\quad + \frac{\eta^7}{12600} - \frac{\eta^6}{240} + \frac{\eta^5}{16} - \frac{13625\eta^2}{252} + \lambda(1-\varepsilon) \\ &\quad \cdot \left. \left(\frac{\eta^6}{240} - \frac{\eta^7}{12600} - \frac{\eta^5}{18} + \frac{125\eta^2}{3} \right) \right] - \frac{a_2}{(1+\epsilon)} \\ &\quad \cdot \left(\frac{\eta^3}{6} - \frac{\eta^4}{120} + \frac{\eta^5}{6000} - \frac{5\eta^2}{4} \right) + \frac{\lambda a_1 \mathrm{Pr} b_1}{(1+\epsilon)} \\ &\quad \cdot \left(\begin{array}{c} (\varepsilon-1) \left(\dfrac{\eta^7}{504000} - \dfrac{\eta^6}{7200} + \dfrac{\eta^5}{120} - \dfrac{5\eta^4}{32} + \dfrac{125\eta^2}{9} \right) \\ +(\gamma - \gamma\varepsilon - \varepsilon) \left(\dfrac{\eta^5}{120} - \dfrac{\eta^6}{720} - \dfrac{5\eta^4}{36} + \dfrac{100\eta^2}{9} \right) \end{array} \right). \end{aligned} \tag{27}$$

$$\begin{aligned} & \theta_2(\eta, b_1, b_2) \\ &= \mathrm{Pr}(1+b_1)b_1 \left[(\varepsilon-1) \left(\frac{\eta^4}{2400} - \frac{\eta^3}{60} + \frac{\eta^2}{2} + \frac{25\eta}{9} \right) \right. \\ &\quad \left. + (\gamma - \gamma\varepsilon - \varepsilon) \left(\frac{\eta^2}{2} - \frac{\eta^3}{60} - \frac{10\eta}{3} \right) \right] + (\mathrm{Pr} b_1)^2 \left[(\varepsilon-1) \right. \\ &\quad \cdot \left(\frac{\eta^6}{14400} - \frac{\eta^7}{1008000} - \frac{\eta^5}{600} + \frac{\eta^4}{64} - \frac{275\eta}{56} \right) \\ &\quad \left. + (\gamma - \gamma\varepsilon - \varepsilon) \left(\frac{\eta^4}{36} - \frac{\eta^5}{600} - \frac{10\eta^3}{9} + \frac{\eta^6}{36000} - \frac{225\eta}{2} \right) \right] \\ &\quad + \frac{\mathrm{Pr} a_1 b_1 (\varepsilon-1)}{(1+\epsilon)} \left[\frac{\eta^7}{1260000} - \frac{\eta^6}{18000} + \frac{\eta^5}{400} - \frac{11\eta^4}{192} \right. \\ &\quad + \frac{5\eta^3}{8} - \frac{7125\eta}{280} + \lambda(1-\varepsilon) \left(\frac{\eta^6}{24000} - \frac{\eta^5}{400} + \frac{\eta^4}{18} \right. \\ &\quad \left. \left. - \frac{5\eta^3}{9} + \frac{625\eta}{30} \right) \right] + \frac{\mathrm{Pr} b_2 (\varepsilon-1)}{10} \left(\frac{\eta^3}{6} - \frac{\eta^4}{240} - \frac{25\eta}{2} \right) \\ &\quad + \mathrm{Pr} b_2 (\varepsilon-1) \left(\frac{\eta^2}{2} - \frac{\eta^3}{30} + \frac{\eta^4}{1200} - \frac{5\eta}{2} \right) + (\gamma - \gamma\varepsilon - \varepsilon) \\ &\quad \cdot \mathrm{Pr} b_2 \left(\frac{\eta^2}{2} - \frac{\eta^3}{60} - \frac{10\eta}{3} \right) + (\mathrm{Pr} b_1)^2 \gamma \left[(\varepsilon-1) \left(\frac{\eta^6}{72000} \right. \right. \\ &\quad - \frac{\eta^5}{1200} + \frac{\eta^4}{24} - \frac{5\eta^3}{8} + \frac{250\eta}{9} \left. \right) + (\gamma - \gamma\varepsilon - \varepsilon) \left(\frac{\eta^4}{24} \right. \\ &\quad \left. \left. - \frac{\eta^5}{1200} - \frac{5\eta^3}{9} + \frac{200\eta}{9} \right) \right] - \frac{\mathrm{Pr} a_1 b_1 \varepsilon}{(1+\epsilon)} \left(\frac{-\eta^6}{72000} \right. \\ &\quad + \frac{\eta^5}{1200} - \frac{\eta^4}{24} + \frac{5\eta^3}{8} - \frac{250\eta}{9} + \lambda(1-\varepsilon) \\ &\quad \cdot \left. \left(\frac{\eta^4}{24} - \frac{\eta^5}{1200} - \frac{5\eta^3}{9} + \frac{200\eta}{9} \right) \right) \end{aligned} \tag{28}$$

The 3rd-order problem:

$$\begin{cases} {f_3}'''(\eta, a_1, a_2, a_3) = (1+a_1){f_2}''' + a_2{f_1}''' + \dfrac{1}{1+\epsilon} \left(\begin{array}{c} a_1 f_0 {f_2}'' + f_1''(a_2 f_0 + a_1 f_1) + f_0''(a_2 f_1 + a_3 f_0) - \sigma \in f_1'' \left(a_2 {f_0'}'^2 + 2a_1 f_0'' f_1'' \right) \\ -\sigma \in a_1 {f_0'}'^2 f_2'' - a_1 \left(2 f_0' f_2' + {f_1'}^2 \right) - 2a_2 f_0' f_1' - a_3 {f_0'}^2 + \lambda(a_1\theta_2 + a_2\theta_1 + a_3\theta_0) \end{array} \right) \\ {\theta_3}''(\eta, b_1, b_2, b_3) = (1+b_4){\theta_2}'' + b_2{\theta_1}'' + \mathrm{Pr} \left[\begin{array}{c} b_3 f_0 {\theta_0}' + b_2 \left(f_0 {\theta_1}' + f_1 {\theta_0}' \right) + b_1 \left(f_0 {\theta_2}' + f_1 {\theta_1}' + f_2 \theta_0' \right) \\ -\left(b_3 f_0' \theta_0 \right) + b_2 \left({f_0}' \theta_1 + {f_1}' \theta_0 \right) + b_1 \left({f_2}' \theta_0 + {f_1}' \theta_1 + f_0' \theta_2 \right) \\ +\gamma(b_1\theta_2 + b_2\theta_1 + b_3\theta_0) - \varepsilon \left(b_1 {f_2}' + b_2 {f'}_1 + b_3 f_0' \right) \end{array} \right] \end{cases} . \tag{29}$$

Table 1: Comparison of results for the skin friction coefficient and Nusselt number for various value of $\varepsilon, \lambda, \sigma$, and E when Pr = 0.7 and $\gamma = 0.1$ are fixed.

E	σ	λ	ε	Present study		Salahuddin et al. [30]	
				Skin friction	$-\theta'(0)$	Skin friction	$-\theta'(0)$
0.1	0.1	0.1	0.1	-0.9948	0.9224	-0.9953	0.9201
0.3	0.1	0.3	0.3	-0.9235	0.9448	-0.9221	0.9450
0.5	0.1	0.5	0.5	-0.8632	0.9661	-0.8629	0.9657
0.1	0.3	0.1	0.1	-0.9987	0.9194	-0.9988	0.9196
0.1	0.5	0.1	0.1	-0.9931	0.9187	-0.9922	0.9192
0.1	0.1	0.3	0.1	-0.8973	0.9482	-0.8969	0.9478
0.1	0.1	0.5	0.1	-0.8046	0.9689	-0.8045	0.9695
0.1	0.1	0.1	0.3	-0.9996	1.0221	-0.9998	1.0216
0.1	0.1	0.1	0.5	-0.8798	1.1223	-0.0043	1.1216

Table 2: Comparison of the present result for local skin friction coefficient and Nusselt number for different values of Pr and ε when $\gamma = \sigma = \lambda = E = 0.1$ are fixed.

Pr	ε	Present result		Bilal and Ashbar [39]		Ogunseye et al. [32]	
		Skin friction	$-\theta'(0)$	Skin friction	$-\theta'(0)$	Skin friction	$-\theta'(0)$
0.1	0.1	-0.954538	0.281633	—	—	-0.954529	0.281631
0.3	0.3	-0.972917	0.524666	-0.972921	0.524669	-0.972908	0.524668
0.5	0.3	-0.985953	0.734565	-0.985951	0.734568	-0.985952	0.734567
0.7	0.5	-0.989286	0.804125	-0.999881	1.021608	-0.989285	0.804125
0.7	0.7	-1.004314	1.121622	−1.004313	1.121621	-1.004309	1.121622
0.7	0.9	-1.008614	1.220177	-1.008613	1.220178	—	—
0.9	1.0	-1.021372	1.237912	—	—	-1.021368	1.237908

Boundary conditions:

$$\begin{cases} f_3(0) = 0, f_3{}'(0) = 0, \theta_3(0) = 0, \\ f_3{}'(\eta) = 0, \theta_3(\eta) = 0 \text{ as } \eta \longrightarrow \infty. \end{cases} \tag{30}$$

Solution for Equation (29) subjected to BCs Equation (30) is achieved in the same way as the zeroth-, first-, and second-order problems. However, there are very bulky expressions to be included herein this paper. Collecting the solution of Equations (21), (24), (28), and (29), we get the four terms solution given as

$$\begin{cases} \tilde{f}(\eta, a_1, a_2, a_3) = f_0(\eta) + f_1(\eta, a_1) + f_2(\eta, a_1, a_2) + f_3(\eta, a_1, a_2, a_3), \\ \tilde{\theta}(\eta, b_1, b_2, b_3) = \theta_0(\eta) + \theta_1(\eta, b_1) + \theta_2(\eta, b_1, b_2) + \theta_3(\eta, b_1, b_2, b_3). \end{cases} \tag{31}$$

4. Result and Discussion

The OHAM is used to solve the transformed nonlinear ODEs describing the problem. The effect of a variety of parameters on skin friction coefficient C_f, Nusselt number Nu, temperature, and velocity has been investigated. The obtained results are displayed with the help of graphical illustrations and tables. Table 1 displays the obtained value of Nu and C_f for particular values of certain parameters and a comparison has been made with published results of others' work. From the table, it is detected that C_f increases with swelling values of the Eyring-Powell fluid material parameter E and mixed convection parameter λ, but it falls off with an augmented value of thermal stratification parameter ε and material fluid parameter σ. It is also found that Nu increases with enhancing mixed convection λ and Eyring-Powell fluid parameter σ.

The impact of the thermal stratification parameter ε and the Prandtl number Pr on Nusselt number Nu and the skin friction coefficient C_f for the fixed value of the other parameters is available in Table 2. The table illustrates C_f is a decreasing function of Prandtl number Pr and the thermal stratification parameter ε. Table 2 also indicates that the local Nusselt number Nu enhances with the increasing value of Pr and ε.

The effect of a variety of parameters on the fluid velocity profile is displayed in Figures 2–7. In Figure 2, the impact of mounting the material parameter E on dimensionless fluid velocity is displayed. The figure points out that the velocity increase with augmenting value of E. Physically, E has an inverse relation with the non-Newtonian fluid's dynamic viscosity. Hence, with increased value of E, the flow resistance reduces, and consequently, the fluid velocity intensifies. Figure 3 is sketched to illustrate the influence of mixed convection parameter λ on velocity profile. It depicts that an intensification in λ results in the rise in the velocity profile. In reality, while fluids are heated their density reduces and buoyancy increases, as a consequence their

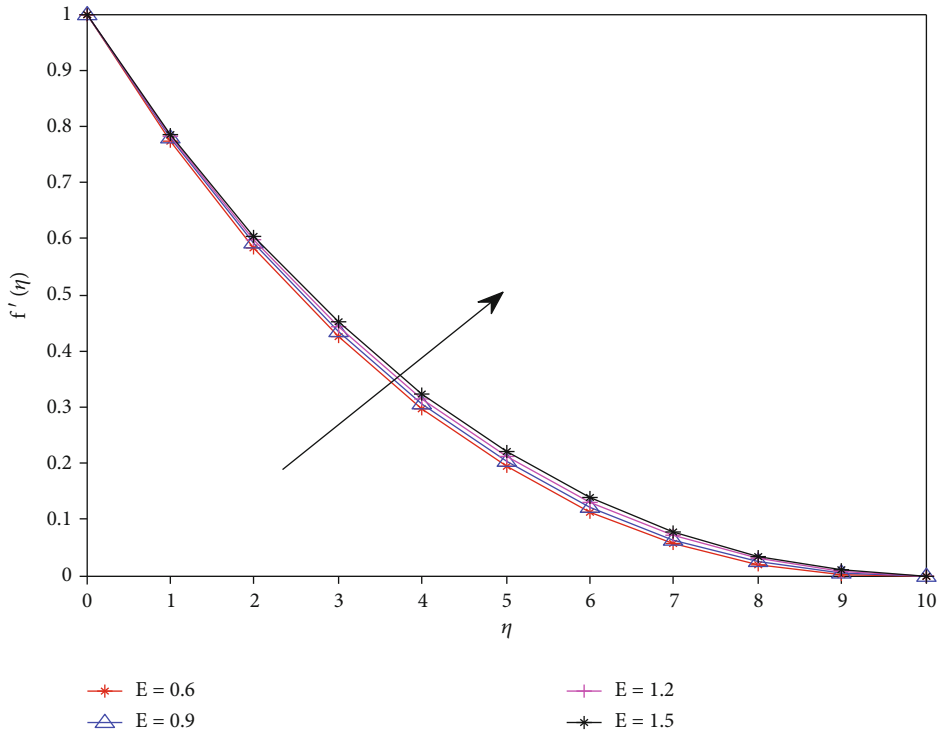

Figure 2: Impact of E on velocity profile when $\lambda = 0.4$,Pr $= 0.72$, $\varepsilon = \sigma = \gamma = 0.1$.

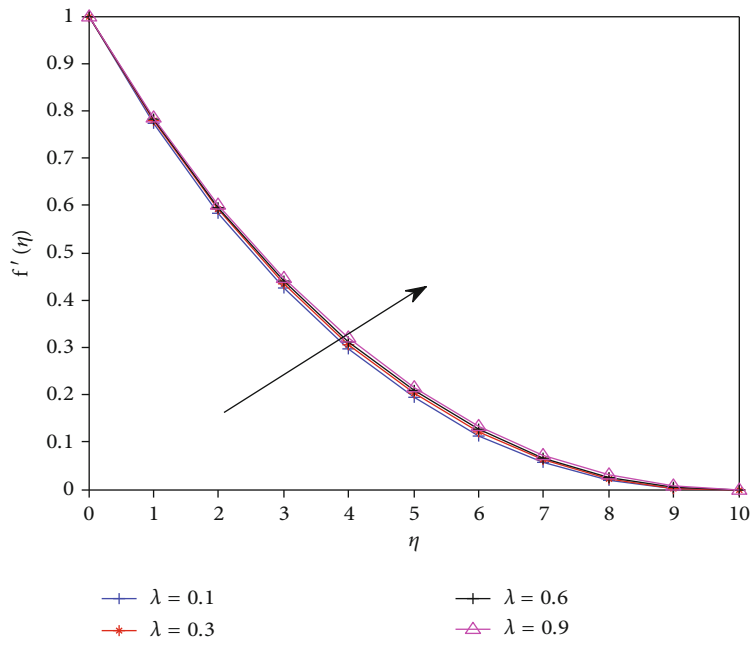

Figure 3: Impact of λ on velocity profile when $E = 0.3$, Pr $= 0.72$, $\varepsilon = \sigma = \gamma = 0.1$.

velocity boosts. Thus, by advancing value λ, one can enhance the velocity within a boundary layer when required.

The influence of thermal stratification parameter ε on the fluid velocity is illustrated in Figure 4. It is witnessed that with higher value of ε, the velocity profile declines. Actually, when ε increases, the convective potential between the heated surface and ambient temperature reduces. The effect of heat generation parameter γ on velocity is exhibited through Figure 5. As can be seen from the figure, the velocity profile enlarges with the value of γ. In reality, while the heat generation parameter rises, additional heat is produced in the fluid; consequently, the fluid turn out to be hotter and less dense, and as a result, its viscosity decreases. Figure 6 displays the effect of material fluid parameter σ on the velocity profile. It is confirmed that the velocity graph increases with the mounting value of σ. In actual fact, σ is inversely related to its viscosity.

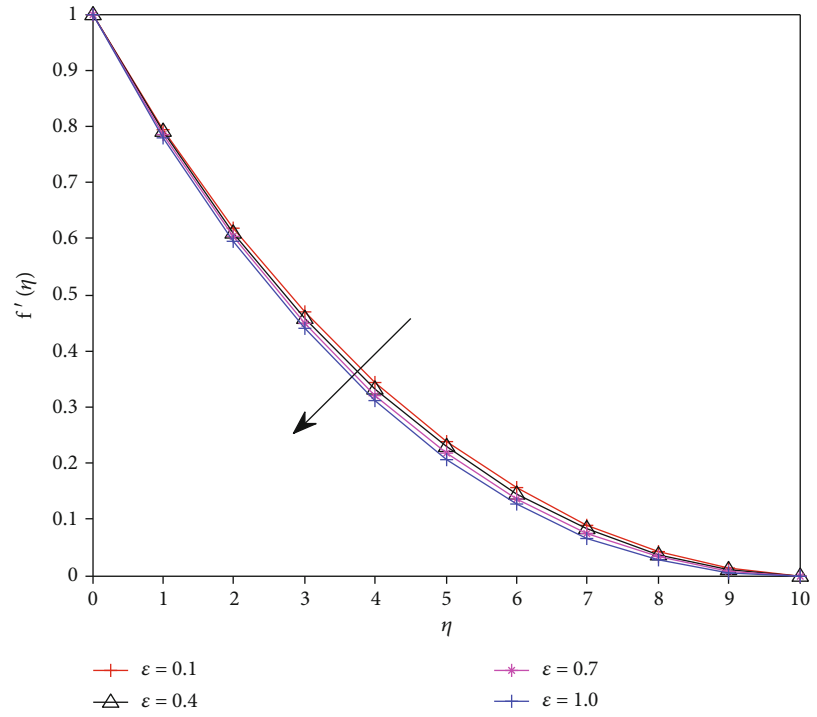

Figure 4: Impact of ε on velocity profile when $\lambda = 0.4$, $E = 0.3$, $\Pr = 0.72$, $\sigma = \gamma = 0.1$.

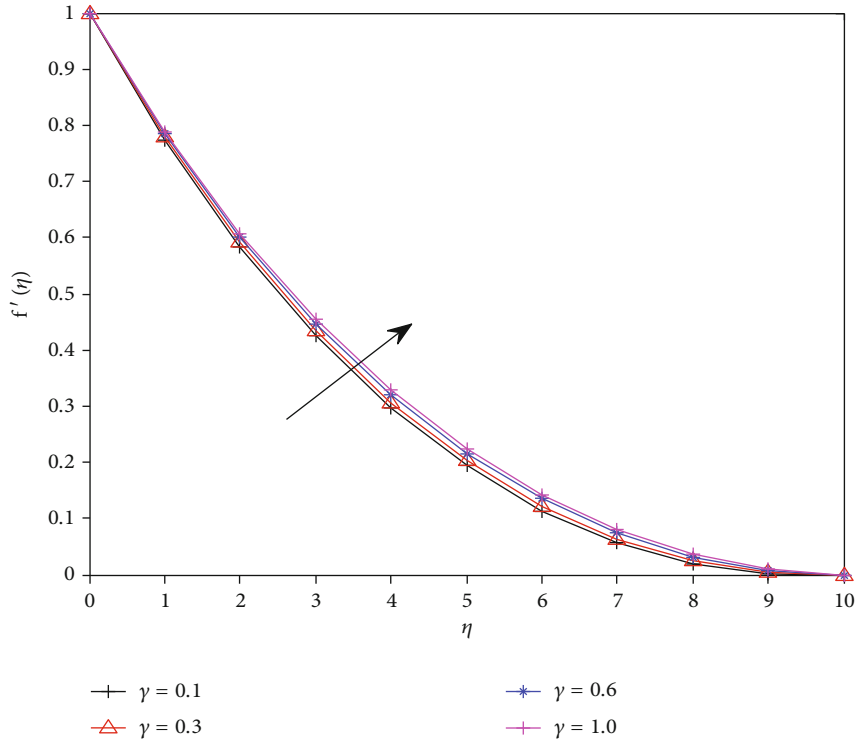

Figure 5: Impact of γ on velocity profile when $\lambda = 0.4$, $E = 0.3$, $\Pr = 0.72$, $\varepsilon = \sigma = 0.1$.

So, the higher the fluid parameter σ leads to the deterioration of the viscous forces; for this reason, the fluid flows rapidly. Figure 7 describes the impact of the Pr on the velocity profile. It is detected that an increment in Pr corresponds to a decrease in the velocity profile of the fluid. Physically, Pr is directly related to the viscosity of the fluid. Because of this fact, as the Pr increases, the fluid turns out to be denser, which causes a decrease in the velocity profile. This may be accredited to the fact that convection currents became diminutive at higher Pr and leads to a decline in velocity.

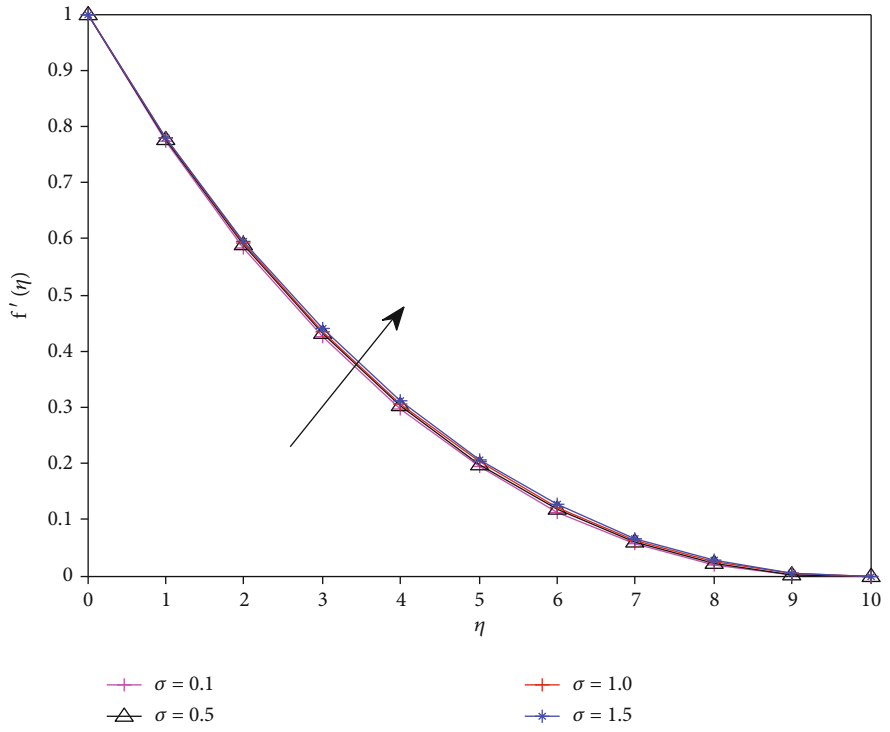

Figure 6: Impact of σ on velocity profile when $\lambda = 0.4$, $E = 0.3$, $\Pr = 0.72$, $\varepsilon = \gamma = 0.1$.

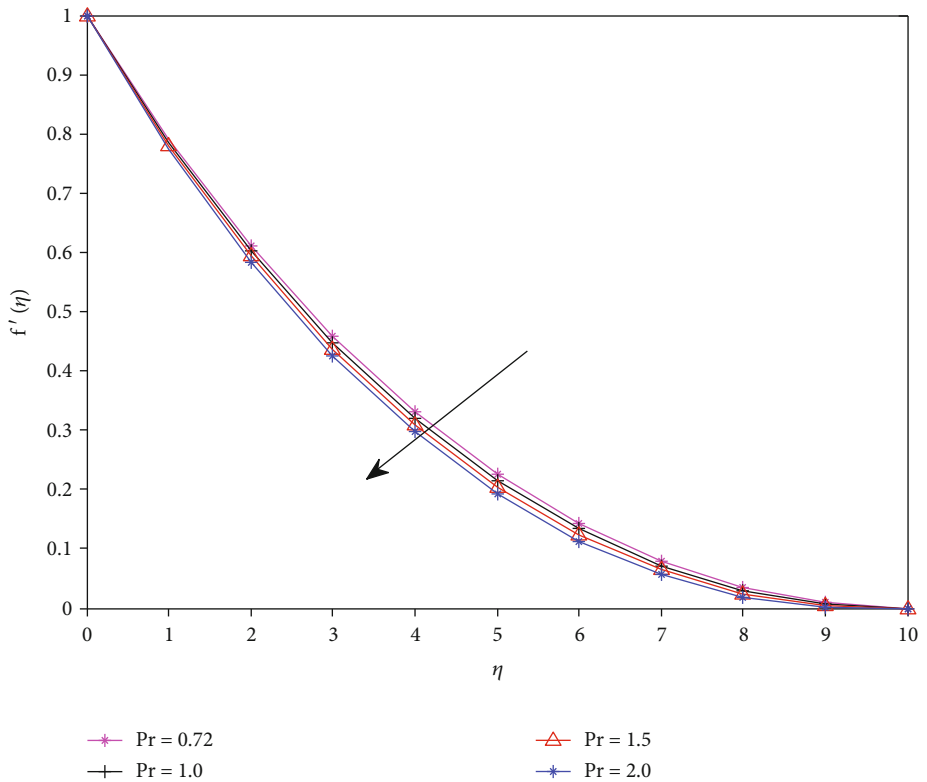

Figure 7: Impact of Pr on velocity profile when $\lambda = 0.4$, $E = 0.3$, $\varepsilon = \sigma = \gamma = 0.1$.

The effect of a variety of parametric quantities on the nondimensional temperature distribution of the fluid under consideration is displayed in Figures 8–13. The characteristic of stratification parameter ε on the temperature is depicted in Figure 8. Physically, the rise in ε declines the temperature distinction between the fluid on the surface and the

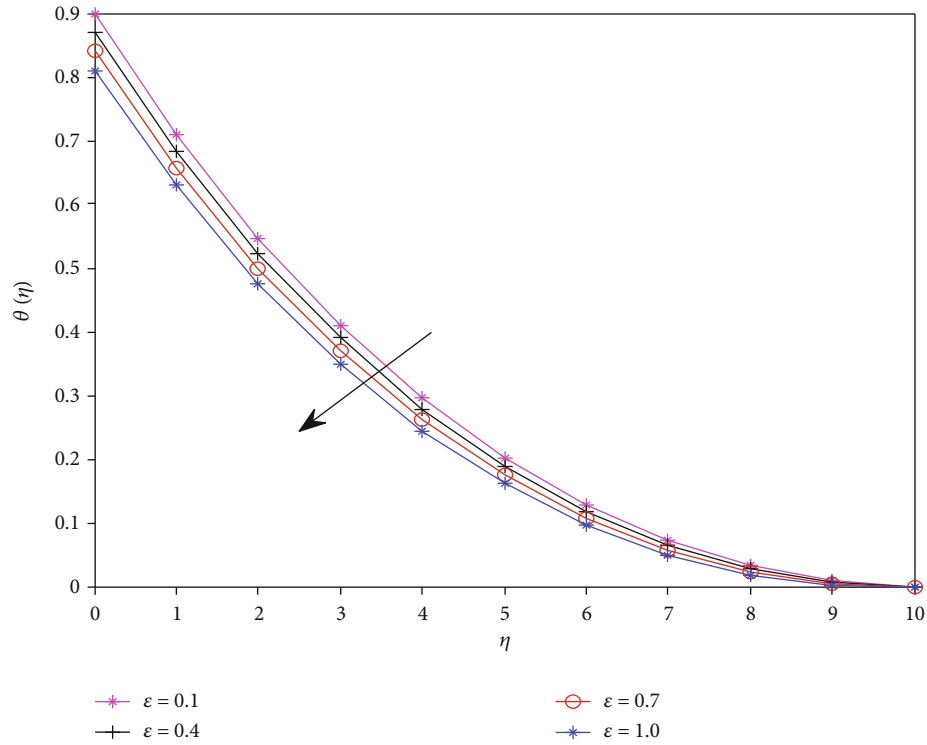

Figure 8: Impact of ε on temperature profile when $\mathrm{Pr} = 0.72$, $\lambda = 0.4$, $E = 0.3$, $\sigma = \gamma = 0.1$.

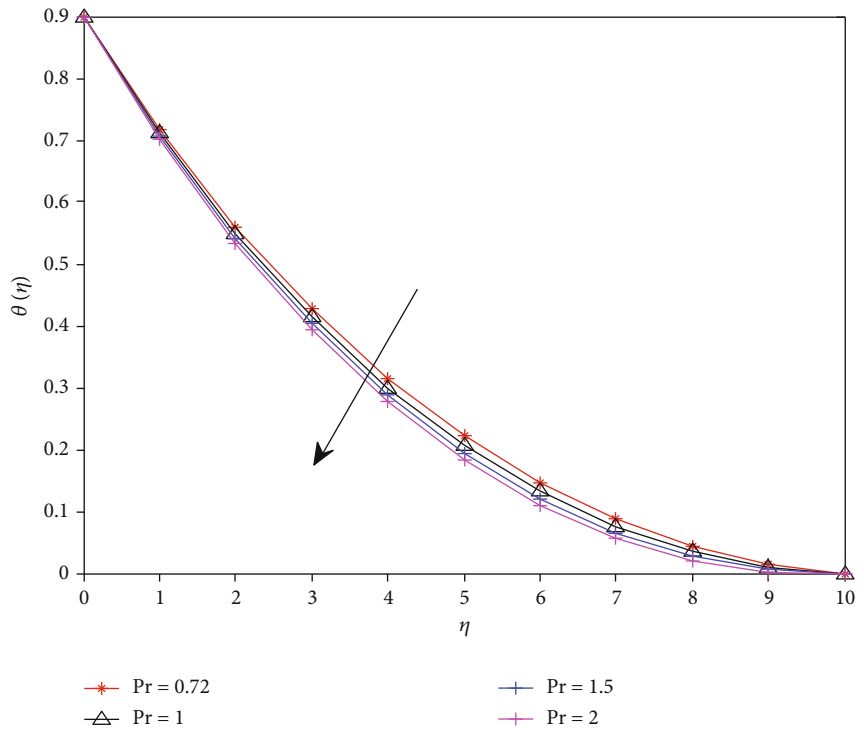

Figure 9: Impact of Pr on temperature profile when $\lambda = 0.4$, $E = 0.3$, $\varepsilon = \sigma = \gamma = 0.1$.

surrounding fluid, this in turn trim down the temperature profile. Thus, the temperature distribution in the fluid drops with an augmentation in the value of ε. Figure 9 reports the effect of the Prandtl number Pr on the temperature profile. It is revealed that when the value of Pr is augmented, the temperature graph reduces. Mathematically, Pr is inversely related to thermal conductivity; hence, the fluid with greater Pr has a low energy diffusion rate. So, the raise in the Pr

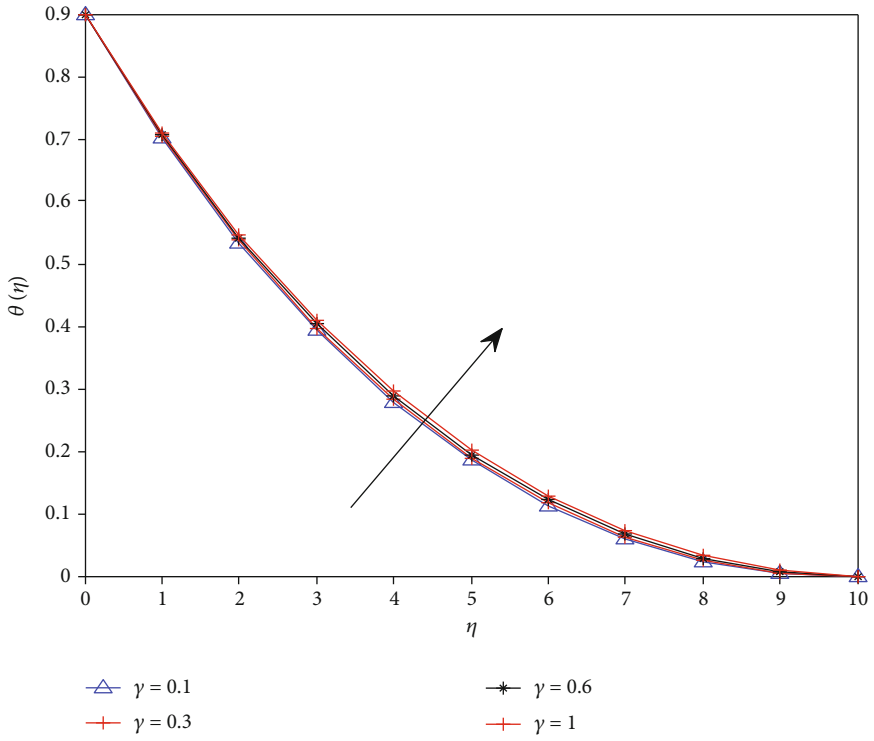

Figure 10: Impact of γ on temperature profile when $\mathrm{Pr} = 0.72$, $\lambda = 0.4$, $E = 0.3$, $\varepsilon = \sigma = 0.1$.

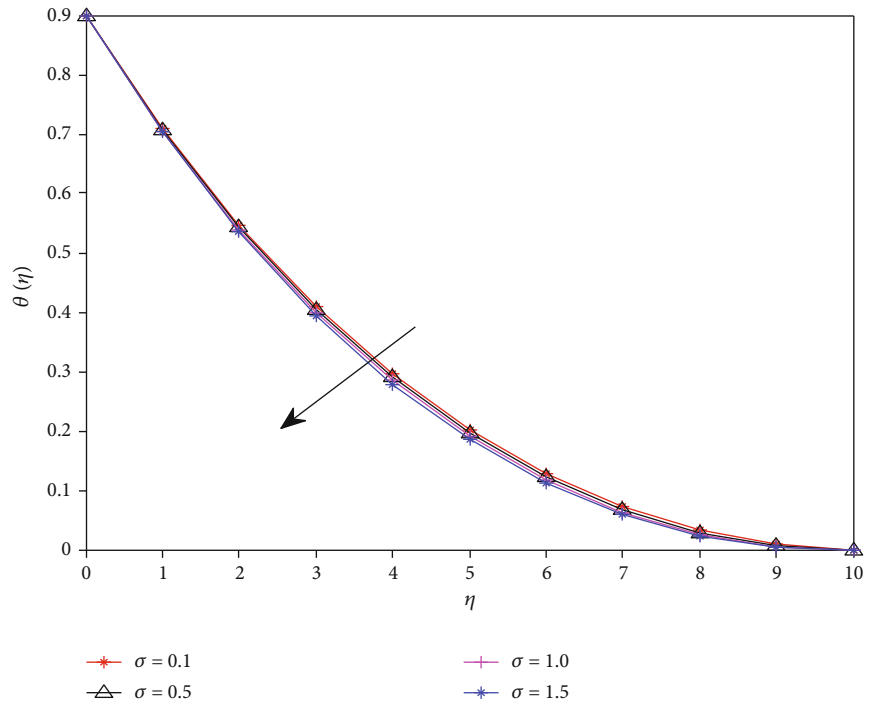

Figure 11: Impact of σ on temperature profile when $\mathrm{Pr} = 0.72$, $\lambda = 0.4$, $E = 0.3$, $\varepsilon = \gamma = 0.1$.

produces a sturdy reduction in the temperature, which upshots the thermal boundary layer thickness. Therefore, in heat transfer, Pr is used to rheostat the thicknesses of thermal and momentum boundary layers.

Figure 10 is plotted to scrutinize the impact of heat generation/absorption parameter γ on the fluid temperature. The figure confirms that when the value γ intensifies, the temperature profile also increases. Physically, higher γ generates extra heat in the fluid system, due to this the temperature profile enhanced. Thus, when the heat generation parameter upshots, considerable heat which can increase the temperature profile of the fluid will be produced.

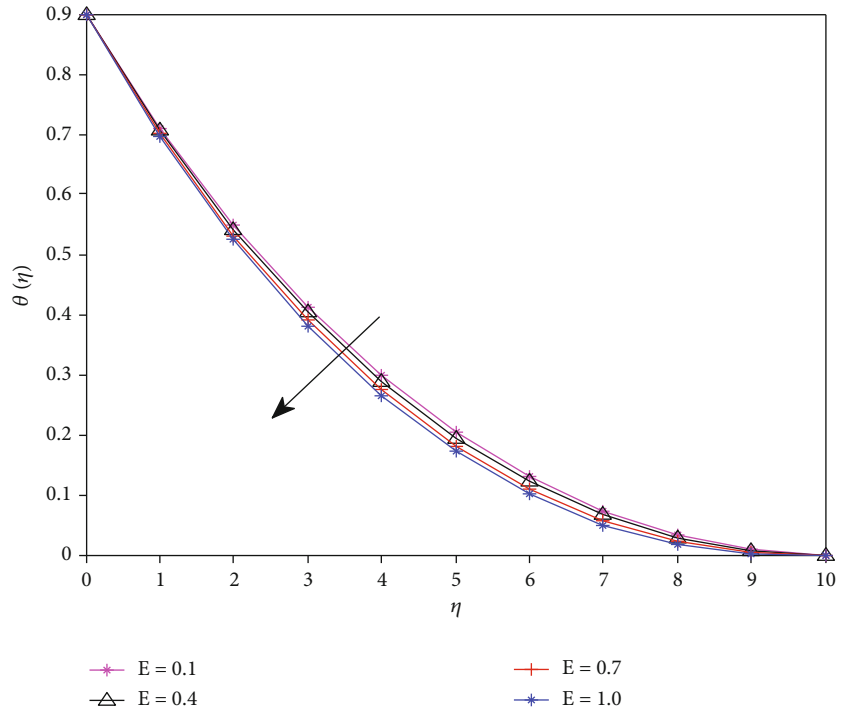

Figure 12: Impact of E on temperature profile when $\Pr = 0.72, \lambda = 0.4, \varepsilon = \sigma = \gamma = 0.1$.

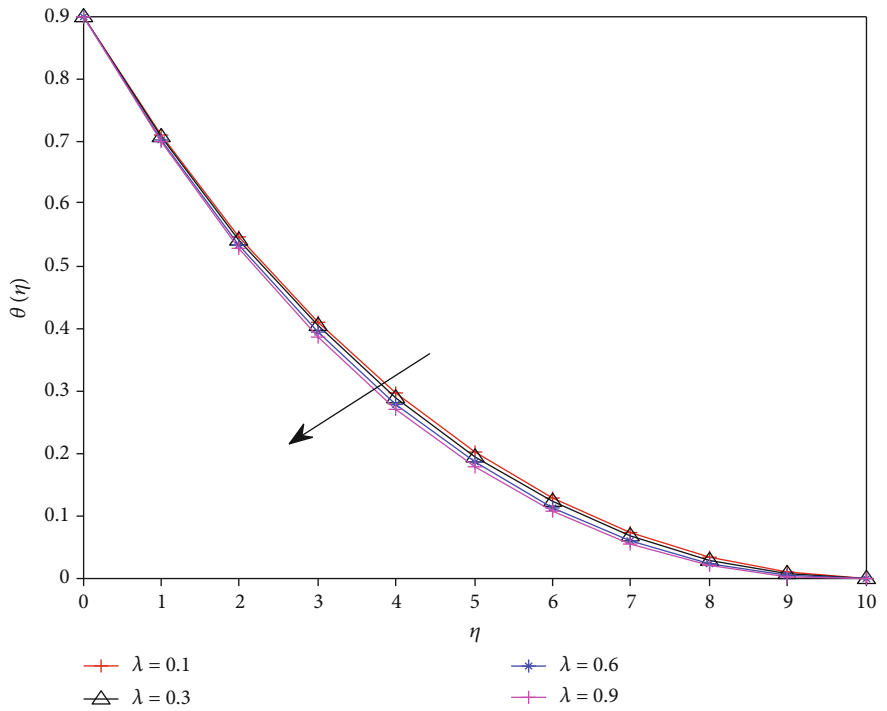

Figure 13: Impact of λ on temperature profile when $\Pr = 0.72, E = 0.3, \varepsilon = \sigma = \gamma = 0.1$.

Therefore, increasing the heat generation/absorption parameter is used to enhance the temperature of the fluid, but sometimes, the augmented values of heat generation parameter results in overmounting in the temperature boundary layer and it should be controlled by using suitable mechanisms.

The characteristic of material fluid parameter σ on the fluid temperature is displayed in Figure 11. It is witnessed that an increment in the value of σ corresponds to a turn down in the temperature profile. This behavior is revealed as σ is inversely associated to the viscosity of the fluid. So,

when σ increases, viscosity reduces which in turn increases the heat transfer rate. Consequently, the temperature of the fluid reduces. Figure 12 portrays the behavior of material parameter E on temperature profile. As we can observe from the figure, an improvement of value of E results in a decrease in the fluid temperature graph. Physically, when E is increased, fluid resistance reduces and contributes to the reduction of temperature distribution. Figure 13 depicts the impact of varied convection parameter λ on temperature. It has been found that when the value of λ increases, the temperature profile declines. This happens attributable to the reduction of the fluid density, as hotter fluids are less dense. Thus, with enhanced value of λ heat transfer rate increases, thereby temperature profile decreases.

5. Conclusion

In this work, we analyze heat transfer and flow of the incompressible, steady Eyring-Powell fluid flow over a two-dimensional stratified prolonging surface with mixed convection. The nonlinear PDEs governing the flow problem and their respective prescribed side conditions have been converted into a couple of nonlinear ODEs via variable similarity transformation and then solved analytically by the OHAM. The quantities of attention in this work are velocity f', temperature θ, skin friction coefficient C_f, and Nusselt number Nu. Thus, the effect of varied parameters embedded in the model on f', θ, C_f, and Nu has been examined and described with the aid of tables and graphs. The main observations drawn from this finding are the following:

(i) With an intensification in value of the thermal stratification parameter ε, both the fluid velocity and the temperature profile decreases. Hence, in various manufacturing processes ε can help to control heat and velocity of fluids

(ii) As the value of the Eyring-Powell fluid material parameter E upsurges, the velocity profile boosts, while the temperature profile declines

(iii) With snowballing values of the mixed convection parameter λ and the material fluid parameter σ, the velocity profile enhances

(iv) As the value of Prandtl number Pr enlarges, the velocity profile dwindles

(v) The temperature distribution turn down with enhancing values of the Prandtl number Pr, the material fluid parameter σ, and the mixed convection parameter λ

(vi) As the value of the heat generation/absorption parameter γ amplifies, both the temperature and the velocity profile increase

(vii) As the values of the mixed convection and the Eyring-Powell fluid material parameters heighten, both the Nusselt number Nu and the skin friction coefficient augment

(viii) With mounting values of the thermal stratification and the material fluid parameters, the skin friction coefficient falloffs

(ix) The local Nusselt number Nu is an increasing function of Prandtl number Pr and the thermal stratification parameter ε, the mixed convection parameter λ, and the Eyring-Powell fluid material parameter E

Abbreviations

a: Linear stretching rate, T^{-1} (1/s)
b_1, b_2: Dimensional constants, QL^{-1}(K/m)
c: Dimensional Eyring-Powell fluid material parameter
c_f: The local skin friction coefficient
c_p: Specific heat of the fluid at a constant temperature, $L^2T^{-2}\theta^{-1}$ (J/kg·K)
e_1: The thermal stratification parameter
f: The dimensionless stream function
g: Gravitational acceleration, LT^{-2} (m/s^2)
k: The fluid thermal conductivity, $MLT^{-3}\theta^{-1}$ (W/m·K)
Nu: Nusselt number
Pr: Prandtl number
Q: Heat generation/absorption coefficient
q_w: Radiation heat flux at the plate surface, MT^{-3} (W/m^2)
T: The fluid temperature, Q (K)
T_0: Stretching sheet reference temperature, Q (K)
T_w: The fluid temperature at the plate surface, Q (K)
T_∞: The temperature far away from the plate surface, Q (K)
u: Velocity component along the x-axis, LT^{-1} (m/s)
u_w: The velocity of the stretching sheet, LT^{-1} (m/s)
v: Velocity component along the y-axis, $[LT^{-1}]$ (m/s)
x, y: Vertical and horizontal coordinate system
η: Dimensionless similarity variable
υ: Kinematic viscosity of the fluid, L^2T^{-1} (m^2/s)
ρ: The fluid density, ML^{-3} (kg/m^3)
β: Dimensional Eyring-Powell fluid material parameter
θ: Dimensionless temperature
ψ: Dimensionless stream function
ε: Material parameter
λ: Mixed convection parameter
γ: Heat generation/absorption parameter, $L\theta^{-2}T^3M^{-1}$ (mK^{2}s^3/kg)
τ: Skin shear stress (N/m^2)
σ: Fluid parameter
∞: Free stream condition
w: Condition at the plate surface.

Data Availability

The data that assist the findings of this work are integrated in the paper.

Conflicts of Interest

The authors declare that they have no conflict of interest.

References

[1] S. Nadeem, S. Ahmad, and N. Muhammad, "Cattaneo-Christov flux in the flow of a viscoelastic fluid in the presence of Newtonian heating," *Journal of Molecular Liquids*, vol. 237, pp. 180–184, 2017.

[2] N. Abbas, S. Saleem, S. Nadeem, A. A. Alderremy, and A. U. Khan, "On stagnation point flow of a micro polar nanofluid past a circular cylinder with velocity and thermal slip," *Results in Physics*, vol. 9, pp. 1224–1232, 2018.

[3] M. Nazeer, M. Farooq Hussain, I. Khan, E. R. El-Zahar, Y.-M. Chu, and M. Y. Malik, "Theoretical study of MHD electro-osmotically flow of third-grade fluid in micro channel," *Applied Mathematics and Computation*, vol. 420, article 126868, 2022.

[4] S. Nadeem and H. Sadaf, "Exploration of single wall carbon nanotubes for the peristaltic motion in a curved channel with variable viscosity," *Journal of the Brazilian Society of Mechanical Sciences and Engineering*, vol. 39, no. 1, pp. 117–125, 2017.

[5] I. Shahzadi, H. Sadaf, S. Nadeem, and A. Saleem, "Bio-mathematical analysis for the peristaltic flow of single wall carbon nanotubes under the impact of variable viscosity and wall properties," *Computer Methods and Programs in Biomedicine*, vol. 139, pp. 137–147, 2017.

[6] J. Wang, M. Ijaz Khan, W. A. Khan, S. Z. Abbas, and M. Imran Khan, "Transportation of heat generation/absorption and radiative heat flux in homogeneous-heterogeneous catalytic reactions of non-Newtonian fluid (Oldroyd-B model)," *Computer Methods and Programs in Biomedicine*, vol. 189, article 105310, 2020.

[7] I. Jabeen, F. Muhammad, R. Muhammad, U. Roman, and A. Shakeel, "Analysis of nonlinear stratified convective flow of Powell-Eyring fluid: application of modern diffusion," *Advances in Mechanical Engineering*, vol. 12, no. 10, 2020.

[8] M. I. Khan, T. Hayat, M. Waqas, and A. Alsaedi, "Outcome for chemically reactive aspect in flow of tangent hyperbolic material," *Journal of Molecular Liquids*, vol. 230, pp. 143–151, 2017.

[9] R. E. Powell and H. Eyring, "Mechanisms for the relaxation theory of viscosity," *Nature*, vol. 154, no. 3909, pp. 427-428, 1944.

[10] Z. Khan, H. U. Rasheed, T. Abbas et al., "Analysis of Eyring–Powell fluid flow used as a coating material for wire with variable viscosity effect along with thermal radiation and Joule heating," *Crystals*, vol. 10, no. 3, p. 168, 2020.

[11] M. S. Upadhay and C. S. Raju, "Cattaneo-Christov on heat and mass transfer of unsteady Eyring Powell dusty nanofluid over sheet with heat and mass flux conditions," *Informatics in Medicine unlocked*, vol. 9, pp. 76–85, 2017.

[12] H. A. Ogunseye and P. Sibanda, "A mathematical model for entropy generation in a Powell-Eyring nanofluid flow in a porous channel," *Heliyon*, vol. 5, no. 5, article e01662, 2019.

[13] S. H. Seyedi, B. N. Saray, and A. J. Chamkha, "Heat and mass transfer investigation of MHD Eyring-Powell flow in a stretching channel with chemical reactions," *Physica A: Statistical Mechanics and its Applications*, vol. 544, article e124109, 2020.

[14] I. M. Eldesoky, S. I. Abdelsalam, W. A. El-Askary, and M. M. Ahmed, "Concurrent development of thermal energy with magnetic field on a particle-fluid suspension through a porous conduit," *BioNanoScience*, vol. 9, no. 1, pp. 186–202, 2019.

[15] M. M. Bhatti, M. Marin, A. Zeeshan, R. Ellahi, and S. I. Abdelsalam, "Swimming of motile gyrotactic microorganisms and nanoparticles in blood flow through anisotropically tapered arteries," *Frontiers of Physics*, vol. 8, p. 95, 2020.

[16] S. I. Abdelsalam and M. M. Bhatti, "Anomalous reactivity of thermo-bioconvective nanofluid towards oxytactic microorganisms," *Applied Mathematics and Mechanics*, vol. 41, no. 5, pp. 711–724, 2020.

[17] Y. A. Elmaboud, S. I. Abdelsalam, K. Mekheimer, and K. Vafai, "Electromagnetic flow for two-layer immiscible fluids," *Engineering Science and Technology, an International Journal*, vol. 22, no. 1, pp. 237–248, 2019.

[18] S. I. Abdelsalamab and K. Vafai, "Combined effects of magnetic field and rheological properties on the peristaltic flow of a compressible fluid in a microfluidic channel," *European Journal of Mechanics-B/Fluids*, vol. 65, pp. 398–411, 2017.

[19] W. Ibrahim and T. Anbessa, "Hall and ion slip effects on mixed convection flow of Eyring-Powell nanofluid over a stretching surface," *Advances in Mathematical Physics*, vol. 2020, Article ID 4354860, 16 pages, 2020.

[20] T. Hayat, M. Waleed Ahmed Khan, A. Alsaedi, and M. Ijaz Khan, "Squeezing flow of second grade liquid subject to non-Fourier heat flux and heat generation/absorption," *Colloid and Polymer Science*, vol. 295, no. 6, pp. 967–975, 2017.

[21] M. I. Khan, S. Qayyum, S. Kadry, W. A. Khan, and S. Z. Abbas, "Irreversibility analysis and heat transport in squeezing nanoliquid flow of non-Newtonian (second-grade) fluid between infinite plates with activation energy," *Arabian Journal for Science and Engineering*, vol. 45, no. 6, pp. 4939–4947, 2020.

[22] M. Ishaq, G. Ali, Z. Shah, S. Islam, and S. Muhammad, "Entropy generation on nanofluid thin film flow of Eyring–Powell fluid with thermal radiation and MHD effect on an unsteady porous stretching sheet," *Entropy*, vol. 20, no. 6, p. 412, 2018.

[23] T. Hayat, R. Sajjad, T. Muhammad, A. Alsaedi, and R. Ellahi, "On MHD nonlinear stretching flow of Powell-Eyring nanomaterial," *Results in physics*, vol. 7, pp. 535–543, 2017.

[24] A. M. Megahed, M. Gnaneswara Reddy, and W. Abbas, "Modeling of MHD fluid flow over an unsteady stretching sheet with thermal radiation, variable fluid properties and heat flux," *Mathematics and Computers in Simulation*, vol. 185, pp. 583–593, 2021.

[25] M. G. Reddy, M. V. V. N. L. Sudha Rani, M. M. Praveen, and K. Ganesh Kumar, "Comparative study of different non-Newtonian fluid over an elaborated sheet in the view of dual stratified flow and Ohmic heat," *Chemical Physics Letters*, vol. 784, article 139096, 2021.

[26] A. M. Megahed and M. Gnaneswara Reddy, "Numerical treatment for MHD viscoelastic fluid flow with variable fluid properties and viscous dissipation," *Indian Journal of Physics*, vol. 95, no. 4, pp. 673–679, 2021.

[27] M. Malik, I. Khan, A. Hussain, and T. Salahuddin, "Mixed convection flow of MHD Eyring-Powell nanofluid over a stretching sheet: a numerical study," *AIP advances*, vol. 5, no. 11, 2015.

[28] J. Rahimi, D. D. Ganji, M. Khaki, and K. Hosseinzadeh, "Solution of the boundary layer flow of an Eyring-Powell non-Newtonian fluid over a linear stretching sheet by collocation

method," *Alexandria Engineering Journal*, vol. 56, no. 4, pp. 621–627, 2017.

[29] M. Zubair, T. Hayat, M. Waqas, A. Alsaedi, and M. Ayub, "On doubly stratified chemically reactive flow of Powell-Eyring liquid subject to non-Fourier heat flux theory," *Results in Physics*, vol. 7, pp. 99–106, 2017.

[30] T. Salahuddin, M. Khan, M. Malik, and F. O. Mallawi, "Change in viscosity of Williamson nanofluid flow due to thermal and solutal stratification," *International Journal of Heat and Mass Transfer*, vol. 126, pp. 941–948, 2018.

[31] T. Hayat, S. Qayyum, M. Imtiaz, and A. Alsaedi, "Double stratification in flow by curved stretching sheet with thermal radiation and joule heating," *Journal of Thermal Science and Engineering Applications*, vol. 10, no. 2, article 021010, 2018.

[32] H. A. Ogunseye, H. Mondal, P. Sibanda, and H. Mambili-Mamboundou, "Lie group analysis of a Powell–Eyringnanofluid flow over a stretching surface with variable properties," *SN Applied Sciences*, vol. 2, 2020.

[33] T.-H. Zhao, M. Ijaz Khan, and Y.-M. Chu, "Artificial neural networking (ANN) analysis for heat and entropy generation in flow of non-Newtonian fluid between two rotating disks," *Mathematical Methods in the Applied Sciences*, 2021.

[34] S. B. Kejela and M. D. Firdi, "Analytical analysis of effects of buoyancy, internal heat generation, magnetic field, and thermal radiation on a boundary layer over a vertical plate with a convective surface boundary condition," *International Journal of Differential Equations*, vol. 2020, Article ID 8890510, 16 pages, 2020.

[35] M. E. Nasr, M. G. Reddy, W. Abbas, A. M. Megahed, E. Awwad, and K. M. Khalil, "Analysis of non-linear radiation and activation energy analysis on hydromagnetic Reiner–Philippoff fluid flow with Cattaneo–Christov double diffusions," *Mathematics*, vol. 10, no. 9, p. 1534, 2022.

[36] V. Marinca and N. Herişanu, "Determination of periodic solutions for the motion of a particle on a rotating parabola by means of the optimal homotopy asymptotic method," *Journal of Sound and Vibration*, vol. 329, no. 9, pp. 1450–1459, 2010.

[37] S. Saleem, S. Nadeem, M. M. Rashidi, and C. S. K. Raju, "An optimal analysis of radiated nanomaterial flow with viscous dissipation and heat source," *Microsystem Technologies*, vol. 25, no. 2, pp. 683–689, 2019.

[38] D. Ibrahim, M. Daba, and S. Bati, "Optimal homotopy asymptotic method for investigation of effects of thermal radiation, internal heat generation, and buoyancy on velocity and heat transfer in the Blasius flow," *Advances in Mathematical Physics*, vol. 2021, Article ID 5598817, 11 pages, 2021.

[39] M. Bilal and S. Ashbar, "Flow and heat transfer analysis of Eyring-Powell fluid over stratified sheet with mixed convection," *Journal of the Egyptian Mathematical Society*, vol. 28, no. 1, pp. 1–16, 2020.

[40] A. Naseem, A. Shafiq, L. Zhao, and M. U. Farooq, "Analytical investigation of third grade nanofluidic flow over a riga plate using Cattaneo-Christov model," *Results in Physics*, vol. 9, pp. 961–969, 2018.